Heliyon 5 (2019) e02252

Contents lists available at ScienceDirect

Heliyon

journal homepage: www.heliyon.com

Effect of extrapallial protein of *Mytilus californianus* on the process of in vitro biomineralization of chitosan scaffolds

S. Jaramillo-Martínez [a], C. Vargas-Requena [a], C. Rodríguez-Gónzalez [b], A. Hernández-Santoyo [c], I. Olivas-Armendáriz [b,*]

[a] Instituto de Ciencias Biomédicas, Universidad Autónoma de Ciudad Juárez, Anillo envolvente del PRONAF y Estocolmo, C.P.32320, Cd. Juárez, Chihuahua, Mexico
[b] Instituto de Ingeniería y Tecnología, Universidad Autónoma de Ciudad Juárez, Ave. Del Charro #610 norte, Col. Partido Romero, C.P.32320, Cd. Juárez, Chihuahua, Mexico
[c] Departamento de Química de Biomacromoléculas, Instituto de Química, Universidad Nacional Autónoma de México, Ciudad de México, Mexico

ARTICLE INFO

Keywords:
Materials science
Bioengineering
Biochemistry
Biotechnology
Materials chemistry
Biomineralization
Chitosan
Extrapaleal protein
Materials application
Materials characterization
Materials processing
Materials property
Materials synthesis

ABSTRACT

Biomineralization is the process by which diverse organisms have the capacity to create heterogeneous accumulations, derived from organic and inorganic compounds that induce the process of mineral formation. An example of this can be seen an extrapallial protein (EP) of *Mytilus californianus*, which is responsible for carrying out the biomineralization process. In order to determine their ability to perform the biomineralization process, EP protein was absorbed and mixed in chitosan scaffolds which were tested in simulated physiological fluid. The materials were analyzed by FTIR spectroscopy, field emission scanning electron microscopy-energy-dispersive electron X-ray spectroscopy andX-ray diffraction. Results confirmed that the EP protein stimulates the rapid growth of biological apatite on the chitosan scaffolds. The mixing method favored more the apatite growth as well as the formation of second nucleation sites than the immersion method.

1. Introduction

Biomaterials present great advantages over those materials commonly used since they do not release cytotoxic products during degradation within biological systems, also their degradation rates can be adjusted by altering the starting formulation or processing conditions [1]. The advantage of these is their innate ability to promote biological recognition, which can positively support cell adhesion and function [2]. Biomaterials of natural origin can be divided into two groups: those based on proteins (for example, collagen, silk fibroin, gelatin, fibronectin, keratin, fibrin and the eggshell membrane) and those based on polysaccharides (for example, hyaluronic acid, cellulose, glucose, alginate, chondroitin, and chitin and its derivative, chitosan). Protein-based biomaterials are typically obtained from animal and human sources and include bioactive molecules that mimic the extracellular environment; while biomaterials based on polysaccharides are mostly obtained from algae, as in the case of agar and alginate, or from microbial sources, such as dextran and its derivatives [3, 4, 5]. For therapeutic applications, these biomaterials are processed for implantation purposes as porous scaffolds, hydrogels, particles, or thin membranes which are *in vivo* enzymatically degradable in non-toxic final products [6].

In recent years, research has been carried out using proteins from materials of marine origin in the manufacture of biomaterials as replacements of bone tissue, which can eventually form biomimetic compounds. These are from 1000 m depth seas; an example of this is the bamboo of the *Isidella* family of corals, which has been investigated by Born and collaborators. They found that the composition of the mineral is responsible for the mechanical stability of the coral, which showed an organic phase of fibrillar acid proteins [7]. On the other hand, the inorganic phase is composed of calcite ($CaCO_3$), so the composition of the skeleton and dimensions of the organic matrix of corals are very similar to the human bone. Another example is described by Rousseau, 2003, in which the biological activity of a water-soluble matrix (WSM) extracted from mother-of-pearl of the bivalve *Pinctada maximal* was studied, with

* Corresponding author.
E-mail address: iolivas@uacj.mx (I. Olivas-Armendáriz).

https://doi.org/10.1016/j.heliyon.2019.e02252
Received 23 December 2018; Received in revised form 4 March 2019; Accepted 5 August 2019

the MC3T2-E1 pre-osteoblast cell line from mice calvaria. Results revealed that the WSM stimulates osteoblast differentiation and osteoid mineralization in 6 days instead of 21 days (period necessary for the mineralization of the osteoid secreted by cells cultured in normal media). This is attributed to acidic glycoproteins present in the WSM [8]. Another bivalve that has been studied is the *Mytilus californianus* of the family of the *Mytilus*, which has an extrapallial space, located between the outside of the epithelial mantle and the growth of the shell, which contains the extrapallial fluid that participates in the process of biomineralization of the mollusk [9]. In this fluid, the mineralization precursors of the shell are concentrated and gathered; they are composed of inorganic substances such as ions of Na^{+}, K^{+}, Mg^{2+}, Ca^{2+}, Cl^{-}, H_2CO_3 (carbonic acid) and sulfates; and by organic substances such as amino acids, mucopolysaccharides, and acids. One of the proteins of the extrapallial fluid that has great importance for being the main cause of the formation of the shell is the extrapallial protein (EP), whose molecular mass is 27.7 kDa and it is the most abundant in said fluid (56%) [10]. It is composed mainly of glutamic acid, which induces the nucleation of calcium ions, thus generating the formation of calcite and aragonite crystals, crystalline structures that constitute the shell of this bivalve [11]. This process of biomineralization resembles bone mineralization; by which it is deduced that this protein carries out activities of calcium fixation, getting to form lamellae or crystals layers [12].

Therefore, the present work determines the effect of the EP protein on chitosan scaffolds; chitosan is a natural polymer widely used in the area of tissue engineering due to its non-toxicity and its properties such as biocompatibility, biodegradability, antimicrobial activity, and healing in wounds [13]. Also, its hydroxyl and carboxyl functional groups allow biological particles to be trapped and act as antibiotics, growth factors, proteins, and bone-forming cells [14]. The scaffolds were manufactured using two protein anchoring methods: absorption and mixing; and different EP concentrations were tested. The scaffolds were exposed to a simulated physiological fluid to determine their capacity to form hydroxyapatite crystals, to identify if the adequate conditions for the *in vitro* biomineralization process occurs.

2. Materials and methods

2.1. Obtaining the extrapallial fluid of Mytilus californianus

The organisms were captured in Baja California, Mexico, and subjected to thermal stress for the EP release; for this, temperatures of 4 and 20 °C were applied at intervals of 4h and 30min, respectively. The collected EP was stored in plastic tubes at −20 °C until use.

2.2. EP purification

The EP was centrifuged at 2,270xg for 15 min; the obtained supernatant was dialyzed at room temperature, using a cellulose membrane with a pore size of 6–8kDa, against 50mM MOPS buffer, pH 7 (3-N-morpholino propanol sulfonic acid), including 0.1M NaCl; this for 24 h with at least three shock absorber replacements, and gentle agitation. The dialyzed sample was centrifuged again at 2,270xg for 15 min; and the supernatant obtained was concentrated to 2.6 mg/mL using an ultrafiltration system (AMICON), with a 10kDa membrane. Subsequently, it was filtered using a membrane with a pore size of 0.22μm and passed, at a flow of 1 mL/min, through a column with anion exchange matrix (Aligent BioWax NP 5, 4.6 × 250mm) previously equilibrated with MOPS-NaCl buffer, in a high resolution system. The fractions were eluted using a linear gradient from 0.1 to 1M NaCl in 50mM MOPS buffer, pH 7. The fractions purity was analyzed by 15% SDS-PAGE and the molecular weight marker was used as a reference for migration. 200 kDa at 6.5kDa (SDS-PAGE Molecular weight Standards BioRad®, Broad Range No. 161-0317). The development of the protein bands was carried out by silver nitrate staining [15].

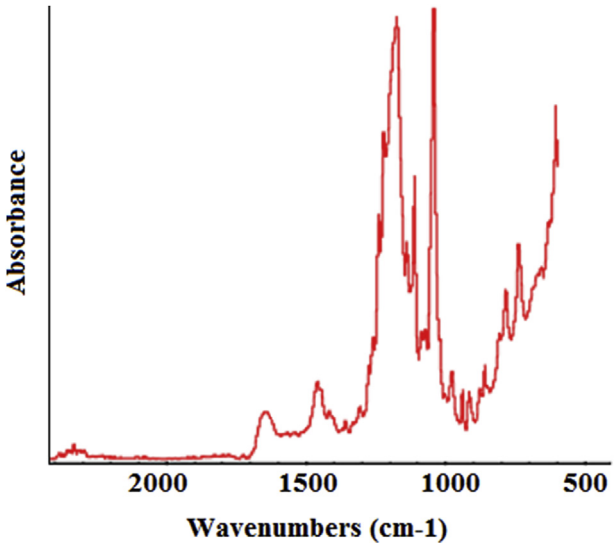

Fig. 1. Infrared spectrum of the pure EP protein.

2.3. Quantification of total protein

For the determination of total protein, the Thermo Fisher kit, PierceTM BCA Protein Assay in microplate was used. This consists in incubating during 30 min at 37 °C, 25μL of the tested sample and 200μL of the BCA reagent; Then the solutions are cooled down for 5 min at room temperature, and their absorbance are measured at 562nm [16]. The calculation of the concentrations was carried out using a standard curve of bovine serum albumin (BSA), at a concentration range of 25–2000 μg/mL. All measurements were made in triplicate with an allowable standard deviation of ±0.05.

2.4. Synthesis of polymer scaffolds

2.4.1. Chitosan scaffold functionalized with EP by absorption

The elaboration of the material was carried out following the method of Olivas-Armendáriz [17], in which 2g of chitosan (85% deacetylation, Sigma-Aldrich) were dissolved in 100mL of a 1% acetic acid solution; this mixture was frozen for 4 h at -40 °C and subsequently lyophilized for 72 h. The material was neutralized with a 0.5% NaOH solution and washed with deionized water. The protein at 50, 100 and 200 μg/mL was added by absorption to material samples of 0.3 mm × 0.5 mm, allowing them to interact for 2 h at room temperature. After this, no protein residues were found suggesting a complete absorption. The scaffolds hereinafter will be identified as chitosan/EP 50 μg/mL A, chitosan/EP 100 μg/mL A, chitosan/EP 200 μg/mL A, the letter A means that the protein was integrated to the scaffolds through absorption.

2.4.2. Chitosan scaffolds functionalized with EP by mixing

The material was prepared by mixing the chitosan solution (prepared as the functionalized scaffolds by absorption) and EP at concentrations of 50, 100 and 200 μg/mL. Once a homogeneous mixture was obtained, the procedure of the EP functionalized scaffolds was continued by absorption. These scaffolds hereinafter will be identified as chitosan/EP 50 μg/mL M, chitosan/EP 100 μg/mL M, chitosan/EP 200 μg/mL M. Where the letter M refers to how the protein was integrated into the scaffolds.

2.5. Bioactivity of scaffolds

A solution of simulated physiological fluid (SBF) was prepared with 1.5 times the ionic concentrations similar to that of blood plasma [18]. Next to the tubes containing the biomaterial functionalized with EP, 5

Table 1
The infrared absorption frequencies (cm^{-1}) of pure EP protein.

Functional group	Wavenumbers (cm^{-1})	Type of vibration
C=O	1750–1550	Stretching
N–H	1562	Bending
–COOH	1324	Stretching
C–H	1315	Vibrations of the protein skeleton
Carbohydrates (C–O and C–O–C)	1350–1010	Stretching/Asymmetric bending
C–N	1186	Stretching
C=O	1070	Stretching
C–N	867	Deformation
N–H	729	Bending
C=O	696	Deformation
C–C	630	Deformation

mL of SBF 1.5X were added and incubated at 37 °C for 7, 14, 21 and 28 days; with the weekly exchange of the SBF to the samples. After the incubation time of the samples, the SBF was removed and dried for 48 h at 37 °C, to then proceed to characterize the material by FT-IR, SEM-EDS, and DRX.

3. Results and discussion

The chemical structure of molecules such as lipids, proteins, carbohydrates, and nucleic acids have components whose chemical bonds have vibrational movements with frequencies within the medium infrared [19]. The FTIR spectra of pure EP (Fig. 1 and Table 1) exhibited absorption bands in a range between 1750 and 1550 cm^{-1}, assigned to C=O stretching vibrations. The bands of N–H bending and –COOH stretching vibration occur in 1562 and 1324 cm^{-1}. C–H vibrations of the protein skeleton are identified by the band at 1315 cm^{-1}. The absorption bands in the region of 1350–1010 cm^{-1} are due to C–O stretching vibrations and C–O–C asymmetric bending. The band at 1186 cm^{-1} revealed that C–N stretching vibration. The absorption bands at 867, 696, and 630 cm^{-1} could be attributed to the presence of C–N and C=O deformation vibrations [19, 20, 21]. All these results suggest the presence of a glycosylated protein.

Fig. 2 shows the infrared spectra of chitosan, chitosan/EP 50 μg/mL A, chitosan/EP 100 μg/mL A, chitosan/EP 200 μg/mL A, chitosan/EP 50 μg/mL M, chitosan/EP 100 μg/mL M, and chitosan/EP 200 μg/mL M scaffolds. Chitosan characteristic bands are observed as the band at 1033 cm^{-1}, which refers to the presence of the ether group (C–O–C); as well as the bands at 1072 cm^{-1} and 1411 cm^{-1} correspond to the stretch of -C–O and the flexure mode of C–H, respectively. The signal at 1562 cm^{-1}

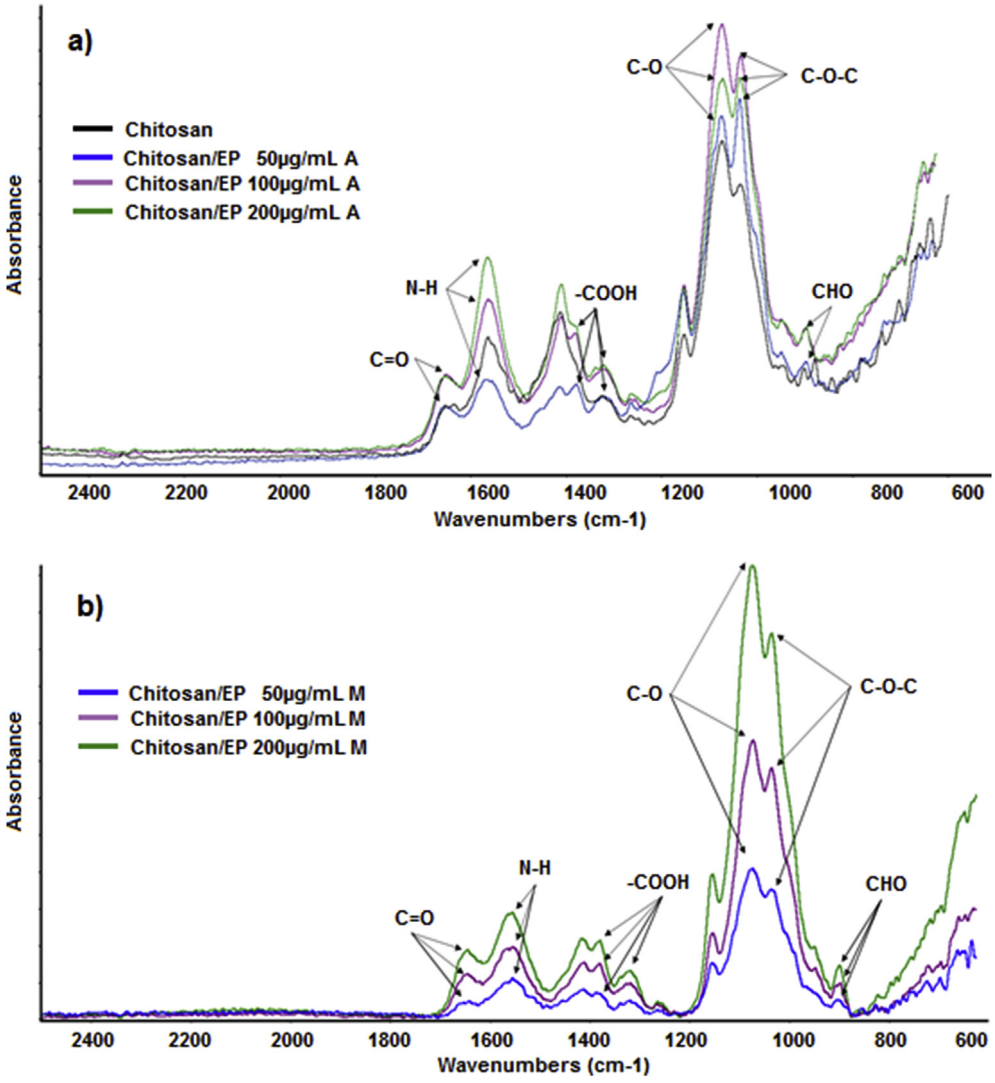

Fig. 2. Infrared spectra of the scaffolds: a) chitosan, chitosan/EP 50 μg/mL A, chitosan/EP 100 μg/mL A, chitosan/EP 200 μg/mL A, b) chitosan EP 50 μg/mL M, chitosan/EP 100 μg/mL M, chitosan/EP 200 μg/mL M.

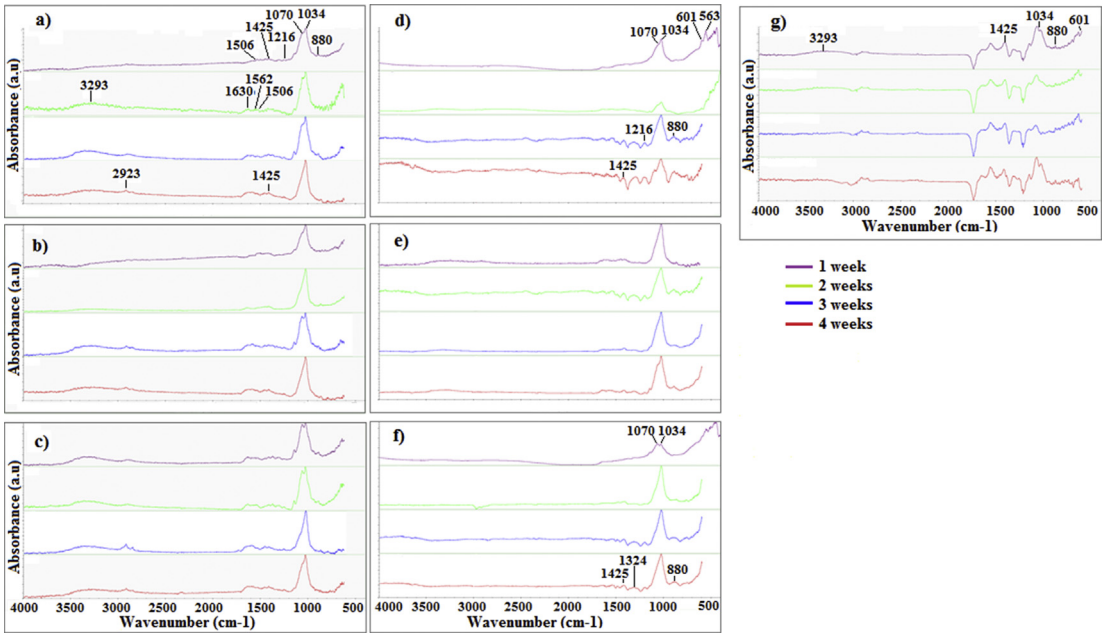

Fig. 3. Infrared spectra of the scaffolds after 4 weeks exposure to the SBF 1.5X solution. Chitosan spectrum (without exposure) was substracted from: a) scaffold of chitosan/EP 50 μg/mL A and b) scaffold of chitosan/EP 50 μg/mL M; c) scaffold of chitosan/EP 100 μg/mL A and d) scaffold of chitosan/EP 100 μg/mL M; e) scaffold of chitosan/EP 200 μg/mL A and f) scaffold of chitosan/EP 200 μG/mL M, and g) scaffold of chitosan.

Table 2
Infrared absorption frecuencies (cm^{-1}) of the treated scaffolds. The original chitosan spectrum was subtracted from each treated scaffold spectrum.

Functional group	Wavenumbers (cm^{-1})	Type of vibration
–OH	3293	Stretching
C=O	1630	Stretching
N–H	1562	Bending
CO_3^{2-}	1506	Stretching
CO_3^{2-}	1425	Stretching
–COOH	1324	Stretching
C–H	1315	Vibrations of the protein skeleton
N–H	1228	Bending
C–O	1216	Stretching
C=O	1070	Stretching
PO_4^{3-}	1034	Bending vibration
CO_3^{2-}	880	Bending vibration
PO_4^{3-}	601	Bending
PO_4^{3-}	563	Bending

corresponds to the bending vibration of the secondary amide (N–H) and the band at 1655 cm^{-1} is attributed to the stretching of the C=O [18]. On the other hand, in the rest of the spectra, it is seen how the characteristic bands of the peptide bond (C=O 1655 cm^{-1} and N–H 1562 cm^{-1}), carboxyls (–COOH 1324 and 1380 cm^{-1}), carbohydrates (C–O 1072 cm^{-1} and C–O–C 1033 cm^{-1}) and saccharide (898 cm^{-1}) [21] increased their intensity with respect to the infrared spectrum of chitosan; in addition to suffer a displacement towards longer wavelengths. These displacements are observed in the infrared spectra of the chitosan/EP 50 μg/mL M, chitosan/EP 100 μg/mL M and chitosan/EP 200 μg/mL M. Peaks were higher as the EP concentration increases in the scaffolds. The results, according to Falini, show the glycosylated protein presence. Meanwhile the displacement of bands to lower wavelengths suggests possible chemical interactions between the chitosan and the protein. The protein has basic aminoacids (arginine, histidine, and lysine) and acidic aminoacids (aspartic acid and glutamic acid) in its polypeptide backbone that present positive and negative charge. Thus, the basic aminoacids (positive charges) interact through electrostatic forces with carboxyl and hydroxyl groups of chitosan (negative charges). These interactions are called saline bonds [21] and allow the anchoring of the protein to the material. On the other hand, the negative charges of the acidic amino acids that constitute the coordination sites are available to interact with calcium and thus conduct the biomineralization process within the material by the nucleation of apatite crystals [22].

The EP functionalized scaffolds after incubation in SBF during 4 weeks were analyzed by FTIR. In order to get a better understanding of the apatite-like layer formation, the original chitosan spectrum was subtracted from each treated scaffold spectrum. Fig. 3 and Table 2 show the FTIR spectra and infrared absorption frequencies of the scaffolds after immersion in SBF for 7, 14, 21, and 28 days. The IR analysis of the scaffolds revealed the presence of bands at 563, 601, and 1034 cm^{-1}, which can be attributed to the bending vibration of the PO_4^{3-} groups. In the same way, inorganic carbonates (CO_3^{2-}) are appreciated at 880, 1427, and 1506 cm^{-1} [23, 24]. This suggests that the formation of phosphate and carbonate crystals was favored. The presence of carbonate and phosphate groups suggests the existence of different calcium phosphates precursors phases of the hydroxyapatite and carbonated hydroxyapatite phases due to the possible substitution of CO_3^{2-} groups by PO_4^{3-} groups. These carbonate species are the most abundant in bones [25]. Bands attributed to the presence of the protein are observed at 1070, 1216, 1228, 1315, 1324, and 1562 cm^{-1} which are related to C=O, C–O, N–H, C–H, –COOH, and N–H groups, respectively. Finally, a band at 3293 cm^{-1} (attributed to the –OH group) is observed. According to El-Hamid and collaborators, it can be attributed to the stretching vibration of the OH hydroxyapatite group [26]. In most of the FTIR spectra, the intensity of the PO_4^{3-} group band remains with the exposure time. However, the C=*O group* band diminished over time. This could be due to the increment of the apatite layer at the scaffold surface [26].

Fig. 4 shows the diffractograms of the chitosan and chitosan scaffolds functionalized with EP (absorption and mixing methods) exposed to the SBF solution during different periods. The chitosan scaffold XRD diffractograms (Fig. 4g) show small peaks reflections since the first week that correspond to the most intense peaks of hydroxyapatite phase (31.7 and 46.7°). After the second week, the hydroxyapatite phase is confirmed by the presence of a third peak at 75.3° [23, 27]. In addition, a peak at 57° and 66° are detected that could relate to the octacalcium phosphate

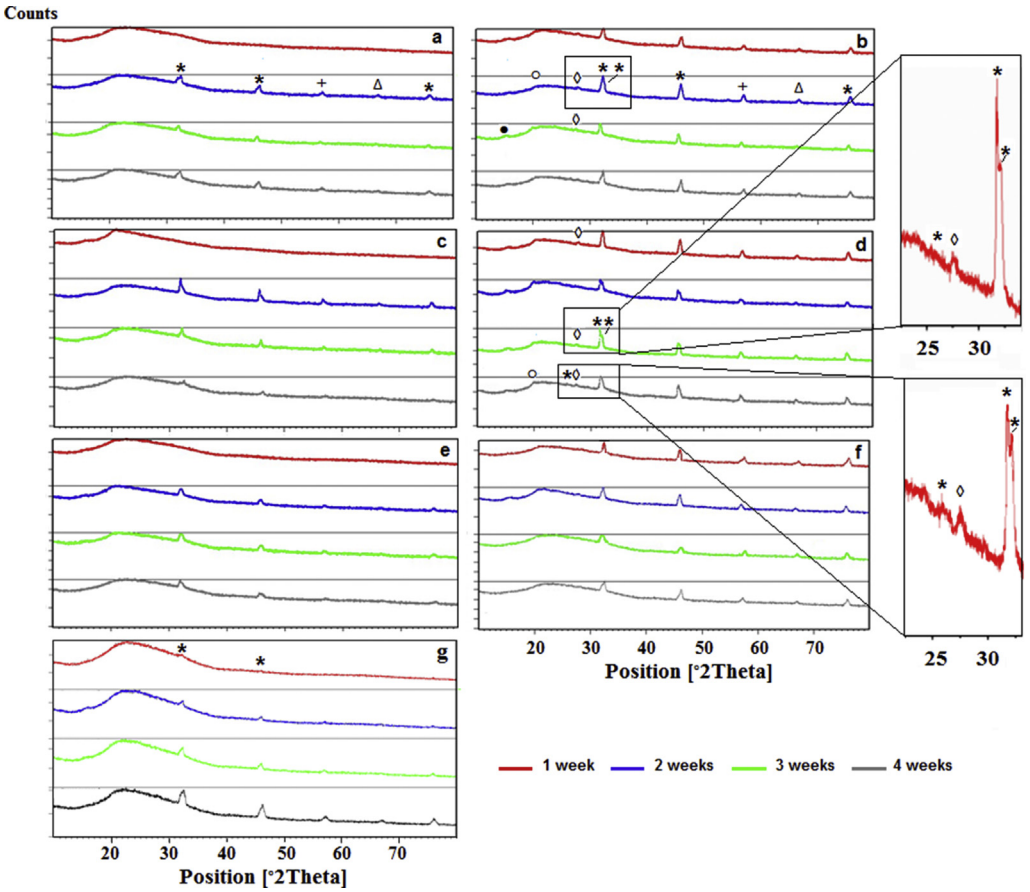

Fig. 4. Diffractogram of the scaffolds at different weeks of incubation in SBF of a) scaffold of chitosan/EP 50 μg/mL A, b) scaffold of chitosan/EP 50 μg/mL M, c) scaffold of chitosan/EP 100 μg/mL A, d) scaffold of chitosan/EP 100 μg/mL M, e) scaffold of chitosan/EP 200 μg/mL A, f) scaffold of chitosan/EP 200 μg/mL M, and g) scaffold of chitosan. * hydroxyapatite, ○ dicalcium phosphate dehydrate, Δ calcium carbonate, + octacalcium phosphate, ◊ β-triclacium phosphate and ● chitosan.

and calcium carbonate crystalline phases [28, 29]. The diffractograms of the functionalized scaffolds by the absorption method showed the presence of crystalline phases after the second week (Fig. 4a, c and e). These phases are the same that the chitosan scaffolds detected phases. During the complete study, the diffractograms of the functionalized scaffolds by mixing exhibit hydroxyapatite peaks at 25.8°, 31.7°, 46.7° and 75.3° [23, 27]. Also, peaks are observed at 19.9° (assigned to dicalcium phosphate dehydrate), 66° (attributed to calcium carbonate), 57° (octacalcium phosphate) and 14° (chitosan) [28, 29]. Fig. 4b and d show the appearance of new peaks at 27.76° and 32.19° (almost overlapping with the peak at 31.7°). These are related to β-tricalcium phosphate and hydroxyapatite, respectively [30]. All XRD results corroborate those obtained by FTIR and suggest the presence of precursors of the hydroxyapatite and carbonated hydroxyapatite phase. More crystalline phases were observed on the functionalized scaffolds by the mixing methodology, suggesting that the nucleation and growth of the apatite crystals were less favored in the scaffolds functionalized by absorption. The above can be attributed to the fact that with the absorption method, the protein may not be homogeneously distributed on the surface of the scaffold, in such a way that the exposure of functional groups such as –COOH responsible for the coordination of Ca^{2+} is limited due to the tendency of the EP to form oligomers. Therefore this effect could be responsible for the loss of its function [31].

The SEM images of the apatite surface formed in the chitosan scaffolds at different periods can be seen in Fig. 5. The microstructure of the apatite layer is similar to the apatite layer formed in materials of CS-coated Ti and Calcium aluminate cement blends when exposed to an SBF solution [25, 32]. In Fig. 5, images of the first week are shown where it is observed how the precipitation occurred through individual granules. During the following weeks of the study, they were gradually accumulated and were filling the pores to form a dense layer on the surface of the scaffolds. The SEM images at higher magnifications (Fig. 6) show how the crystals agglomerate to form a continuous layer in the form of spheres, similar to cauliflower morphology, already reported by [23]. Several investigations report that the symmetry of the crystals could be mediated by the interaction of proteins with calcium ions through negatively charged amino acids; causing the conglomeration of crystals and their growth [21, 22].

On the other hand, all the scaffolds, as the incubation time increases, the formation and deposition of apatite crystals increase on their surface. However, the formation of crystals also occurs in the chitosan scaffolds; these are generated by the own salts that integrate the solution of SBF; appearing in smaller quantity in comparison with the scaffolds containing EP. When analyzing materials according their manufacturing technique and concentration of EP, it is observed that the scaffolds of chitosan/EP 50 μg/mL A and chitosan/EP 100 μg/mL M (scaffolds where the protein anchoring was by absorption and mixing) present a greater deposition of crystals throughout their entire surface during the complete study. However, the scaffolds of chitosan/EP 100 μg/mL M was the one where deposition and growth of apatite crystals cover a greater percentage of the surface compared to the chitosan/EP 50 μg/mL A scaffold and the rest of the scaffolds. It even showed second nucleation sites when growing on top of each other, and entering the pores of the chitosan. Because of this, the porous morphology of the scaffolds after the 3rd week of the study was not observed. These results can be attributed to the fact that the mixing technique allowed greater interaction between

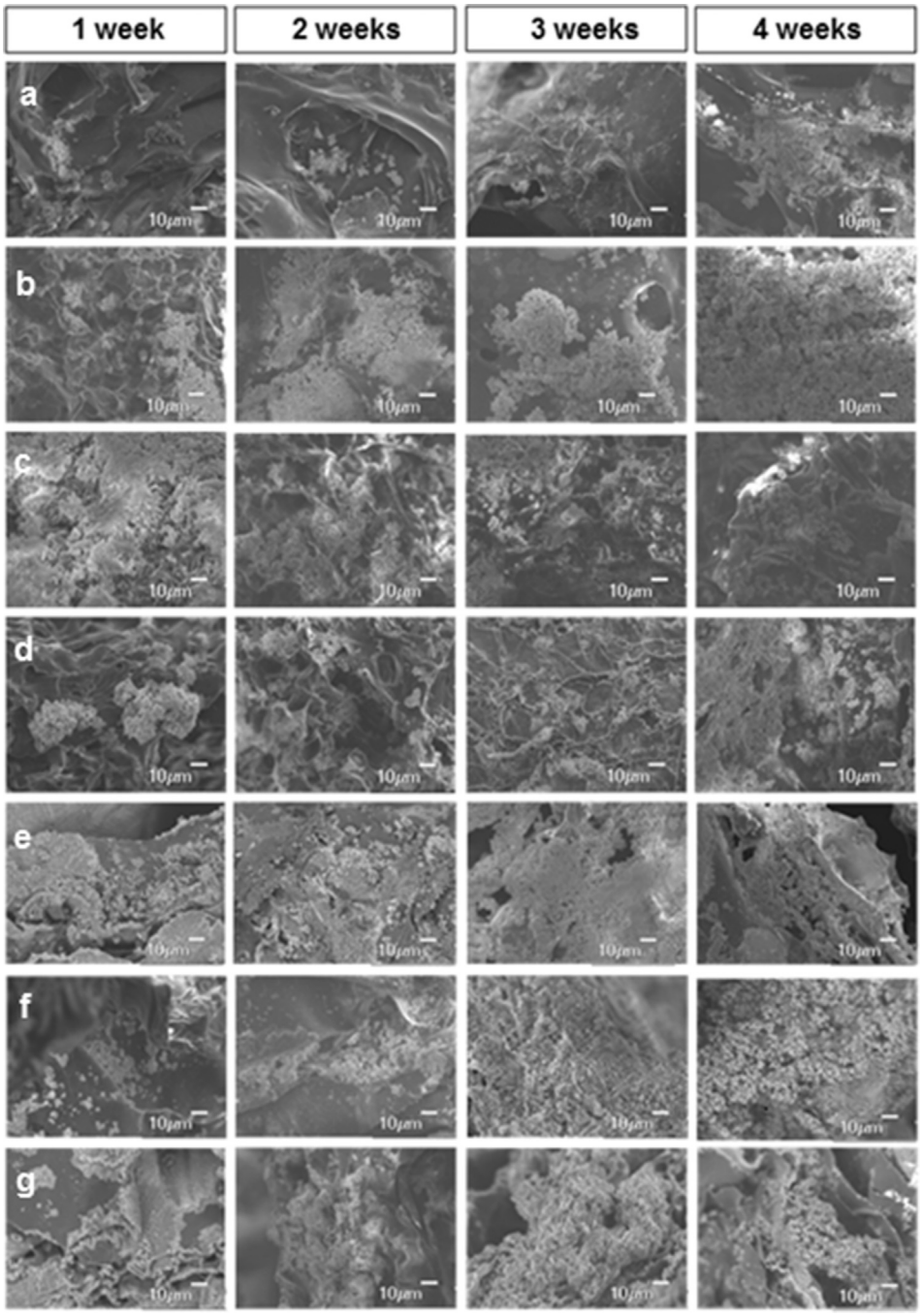

Fig. 5. SEM images of the scaffolds: a) chitosan, b) chitosan/EP 50 μg/mL A, c)chitosan/EP 100 μg/mL A, d) chitosan/EP 200 μg/mL A e) chitosan/EP 50 μg/mL M, f) chitosan/EP 100 μg/mL M, g) chitosan/EP 200 μg/mL M after soaking in SBF.

chitosan-EP, resulting in a more homogeneous sample with regard to the placement and exposure of EP functional groups. On the other hand, in the SEM images of the chitosan/EP 200 μg/mL M scaffold, it is observed how the crystallization process was hindered by containing 200 μg/mL of PE. This is attributed to the fact that as the concentration of the protein favors the protein-protein interaction [22], an effect that could be hindering to adequate nucleation and consequently, the growth of crystals.

EDS analyses are shown in Table 3 and Fig. 6. Elements such as calcium and phosphorus are observed. Their presence is related to the formation of calcium phosphate phases, such as hydroxyapatite [25]. In addition to elements such as carbon, oxygen, silver, sodium, and magnesium, is the carbon a component of the scaffolds and silver due to the sample preparation. Table 2 shows how the Ca/P atomic ratio was increased in all scaffolds throughout the exposure time being found during the first week at 1.30, 1.29, 1.46, 1.27, 1.31, 1.24, and 1.23 for the scaffolds of chitosan/EP 50 μg/mL A, chitosan/EP 100 μg/mL A, chitosan/EP 200 μg/mL A chitosan/EP 50 μg/mL M, chitosan/EP 100 μg/mL M, chitosan/EP 200 μg/mL M and chitosan, respectively. Atomic ratios that agree with calcium deficient apatite (1.33–1.66, variable) and amorphous calcium phosphate (1.2–2.2, variable) [30]. At the end of the fourth week (in all the scaffolds), a Ca/P relation related to the formation of apatite layers deficient in calcium was obtained. Also, higher Ca/P atomic ratios were observed in the scaffolds functionalized by absorption since in most periods of studies, atomic relationships similar to apatite

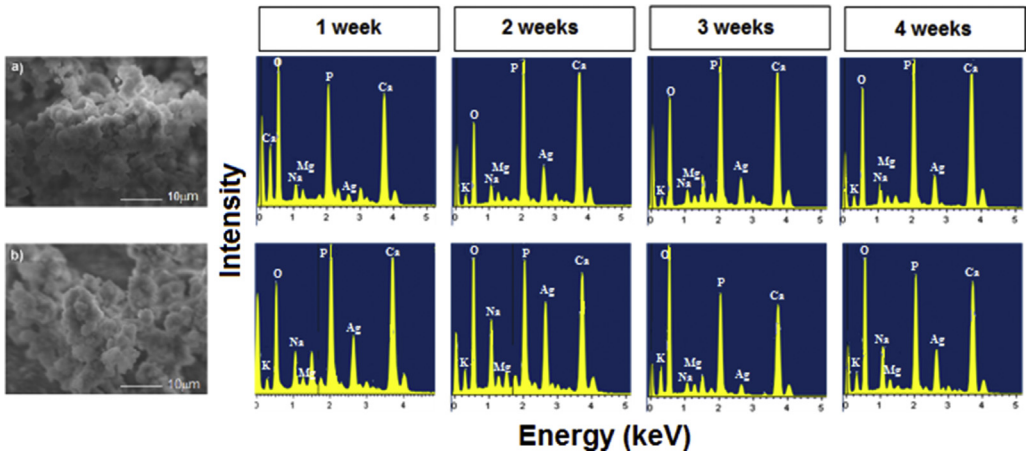

Fig. 6. Images of SEM and EDS spectrum of the apatite layer formed on the scaffolds of a) quitosana/EP 50 µg/mL A y b) quitosana/EP 100 µg/mL M after soaking in SBF.

Table 3
Ca/P atomic ratio of the surface of HA after soaking time in SBF.

Sample/soaking time in SBF (week)	1	2	3	4
Chitosan/EP 50 µg/mL A	1.30	1.36	1.36	1.57
Chitosan/EP 100 µg/mL A	1.29	1.53	1.40	1.54
Chitosan/EP 200 µg/mL A	1.46	1.50	1.37	1.59
Chitosan/EP 50 µg/mL M	1.27	1.29	1.34	1.44
Chitosan/EP 100 µg/mL M	1.31	1.26	1.27	1.32
Chitosan/EP 200 µg/mL M	1.24	1.31	1.36	1.40
Chitosan	1.23	1.34	1.32	1.36

and closer to the atomic ratio Ca/P of hydroxyapatite were obtained. The chitosan scaffold and scaffolds in which the polymer was mixed with the protein, these values were slightly lower. These results suggest that the crystals formed on the surface of the material are apatite deficient in calcium or carbonated, which is also confirmed by FTIR and DRX, which showed that the carbonate groups partially replace the phosphate groups. On the other hand, researchers like Ohtsuki have reported that in layers of surface apatite that contain small amounts of Na and Mg, as well as large amounts of Ca and P, Mg could replace Ca in the apatite crystal, obtaining an apatite crystal similar to bone [33]. Concerning the role of EP, the results obtained in the different characterizations analyses made, indicate that it plays an important role in the apatite nucleation on the scaffold surface.

Fig. 7 illustrates the cross section BSE-SEM images of chitosan/EP 100 µg/mL M scaffolds soaked in SBF for 7, 14, 21, and 28 days. Bright phase spots are observed that are due to the deposit of apatite particles inside the interconnected porosity (revealed with the cross-sectional cut). The apatite deposits in the pores increase with the SBF exposure time. The EDX analyses of the cross sections showed the presence of the same elements detected on the samples surfaces (Fig. 6).

4. Conclusion

Chitosan/EP scaffolds were successfully synthetized by "Thermally Induced Phase Separation (TIPS)," and EP protein was added using immersion and mixing methods. The findings support the EP plays an important role in facilitating the apatite nucleation on the scaffold surface. Apatite-like layer formation was observed on the surfaces and inside the connected porosity of scaffolds after SBF immersion. The apatite formation and the *in vitro* biomineralization process is more favored when the mixing functionalization methodology is used. These EP functionalized scaffolds could offer a potential improvement of osseointegration in future in-vivo applications.

Declarations

Author contribution statement

Silvia Jaramillo-Martínez & Claudia Vargas: Conceived and designed the experiments; Performed the experiments; Wrote the paper.

Claudia Rodriguez: Conceived and designed the experiments; Wrote the paper.

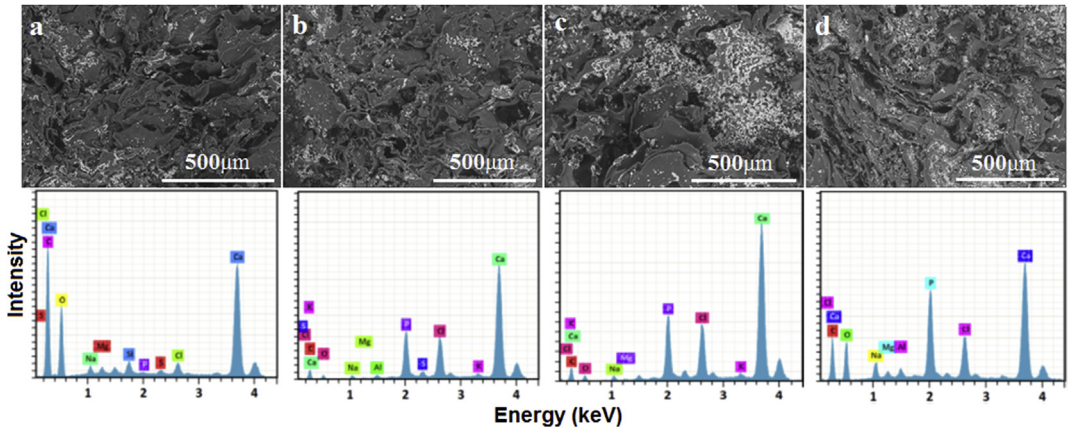

Fig. 7. Cross section BSE-SEM images of chitosan/EP 100 µg/mL M scaffolds soaked in SBF for (a)1, (b) 2, (c) 3, and (d) 4 weeks.

Alejandra Hernandez-Santoyo: Performed the experiments; Contributed reagents.

Imelda Olivas-Armendariz: Conceived and designed the experiments; Performed the experiments; Analyzed and interpreted the data; Contributed reagents, materials, analysis tools or data; Wrote the paper.

Funding statement

This work was supported by the Mexican National Council for Science and Technology (SEP-CONACyT CB 2015-01-252439).

Competing interest statement

The authors declare no conflict of interest.

Additional information

No additional information is available for this paper.

References

[1] W. Stoppel, C. Ghezi, A.R. McNamara, L. Iii, D. Kaplan, Erratum to clinical applications of naturally derived biopolymer-based scaffolds for regenerative medicine, Ann. Biomed. Eng. 43 (2015) 2023.
[2] A. Rent, M. Detamore, Leveraging "raw materials" as building blocks and bioactive signals in regenerative medicine, Tissue Eng. B Rev. 18 (2012) 341–362.
[3] D. Chow, M. Nunalee, D. Lim, A. Simnick, A. Chilkoti, Peptide-based biopolymers in biomedicine and biotechnology, Mater. Sci. Eng. R Rep. 62 (2008) 125–155.
[4] F. Cui, Y. Li, J. Ge, Self- assembly of mineralized collagen composites, Mater. Sci. Eng. R Rep. 15 (2007) 1–27.
[5] J. Mano, G. Silva, H. Azevedo, P. Malafaya, S. Silva, L. Boesel, R. Reis, Natural origin biodegradable systems in tissue engineering and regenerative medicine: present status and some moving trends, J. R. Soc. Interface 4 (2007) 999.
[6] P. Zarrintaja, S. Manouchehria, Z. Ahmadib, M. Reza Saebc, A. Urbanskad, D. Kaplane, M. Mozafarif, Agarose-based biomaterials for tissue engineering, Carbohydr. Polym. 187 (2018) 66–84.
[7] R. Born, H. Ehrlich, V. Bazhenov, N. Shapkin, Investigation of nanoorganized biomaterials of marine origin, Arab. J. Chem. 3 (2010) 27–32.
[8] M. Rousseau, L. Pereira-Mouriès, M. Almeida, C. Milet, E. Lopez, The water-soluble matrix fraction from the nacre of Pinctada maxima produces earlier mineralization of MC3T3-E1 mouse pre-osteoblasts, Comp. Biochem. Physiol. B Biochem. Mol. Biol. 135 (2003) 1–7.
[9] T. Takehuchi, I. Sarashina, M. Iijima, E. Kazuyoshi, In vitro regulation of CaCO3 crystal polymorphism by the highly acidic molluscan shell protein Aspein, FEBS Lett. 582 (2008) 591–596.
[10] R. Salazar-Vázquez, Estudio de una proteína involucrada en la formación de la concha de *Mytilus edulis* y su relevancia en la biomineralización, Maestría en Ciencias Orientación Genómica, Universidad Autónoma de Ciudad Juárez, Ciudad Juárez, Chihuahua, 2011.
[11] G. Jalife-Chavira, Estudio biofísico y estructural de la proteína extrapaleal de *Mytilus edulis* y su participación en el proceso de biomineralización, Maestría en Ciencias Orientación Genómica, Universidad Autónoma de Ciudad Juárez, Ciudad Juárez, Chihuahua, 2012.
[12] J. Roqué, J. Molera, M. Vendrell. Saz, N. Salvadó, Crystal size distributions of induced calcium carbonate crystals in polyaspartic acid and *Mytilus edulis* acidic organic proteins aqueous solutions, J. Cryst. Growth 262 (2003) 543–553.
[13] D. Wang, Y. Zhang, Z. Hong, Novel fast-setting chitosan/β-dicalcium silicate bone cements with high compressive strength and bioactivity, Ceram. Int. 40 (2014) 9799–9808.
[14] Q. Chen, S. Cabanas-Polo, O. Goudouri, A. Boccaccini, Electrophoretic deposition of antibiotic loaded PHBV microsphere-alginate composite coating with controlled delivery potential, Colloids Surfaces B Biointerfaces 130 (2015) 199–206.
[15] C.R. Merril, R. Switzer, M. Van Keuren, Trace polypeptides in cellular extracts and human body fluids detected by two-dimensional electrophoresis and a highly sensitive silver stain, Proc. Natl. Acad. Sci. 76 (1979) 4335–4339.
[16] P. Smith, R. Krohn, G. Hermanson, A. Mallia, F. Gartner, M. Provenzano, E. Fujimoto, N. Goeke, B. Olson, D. Klenk, Measurement of protein using bicinchoninic acid, Anal. Biochem. 150 (1985) 76–85.
[17] I. Olivas-Armendáriz, P. García-Casillas, R. Martínez-Sánchez, A. Martínez-Villafañe, C.A. Martínez-Pérez, Chitosan/MWCNT composites prepared by thermal induced phase separation, J. Alloy. Comp. 495 (2010) 592–595.
[18] S.A. Martel-Estrada, C.A. Martínez Pérez, J. Chacón, P.E. García-Casillas, I. Olivas-Armendariz, In vitro bioactivity of chitosan/poly (d,l-lactide-co-glycolide) composites, Mater. Lett. 65 (2011) 137–141.
[19] G. Barraza-Garza, L.A. de la Rosa, A. Martínez-Martínez, H. Castillo-Michel, M. Cotteb, E. Alvarez-Parrilla, La microespectroscopía de infrarrojo con transformada de Fourier (FTIRM) en el estudio de sistemas biológicos, Rev. Latinoamer. Quím. 41 (2013) 3.
[20] G. Viruthagiri, P. Pravee, S. Mugunda, M. Anbuvanna, Growth and characterization of L-histidine doped thiourea single crystals by slow evaporation method, Indian J. Adv. Chem. Sci. 1 (4) (2013) 193–200.
[21] G. Falini, G. Sartor, D. Fabbri, P. Vergni, S. Fermani, A. Belcher, G. Stucky, D. Morse, The interstitial crystal-nucleating sheet in molluscan Haliotis rufescens shell: a bio-polymeric composite, J. Struct. Biol. 173 (2011) 128–137.
[22] S. Hattan, T. Laue, N. Chasten, Purification and characterization of a novel calcium-binding protein from the extrapallial fluid of the mollusk, *Mytilus edulis*, J. Biol. Chem. 276 (2011) 4461–4468.
[23] S.A. Martel-Estrada, I. Olivas-Armendáriz, E. Santos-Rodríguez, C.A. Martínez-Pérez, P.E. García-Casillas, J. Hernández-Paz, C.A. Rodríguez-González, C. Chapa-González, Evaluation of in vitro bioactivity of Chitosan/Mimosa tenuiflora composites, Mater. Lett. 119 (2014) 146–149.
[24] G. Chouzouri, M. Xanthos, In vitro bioactivity and degradation of polycaprolactone composites containing silicate fillers, Acta Biomater. 3 (2007) 745–756.
[25] I.R. de Oliveira, L.J. Raniero, V.M.C. Leite, L.M.S. Castro-Raucci, P.T. de Oliveira, V.C. Pandolfelli, In vitro apatite-forming ability of calcium aluminate blends, Ceram. Int. 43 (2017) 10071–10079.
[26] K.H. Kim, T. Himeno, M. Kawashita, T. Kokubo, T. Nakamura, The mechanism of biomineralization of bone-like apatite on synthetic hydroxyapatite: an in vitro assessment, J. R. Soc. Interface 1 (2004) 17–22.
[27] S. Jebri, I. Khattech, M. Jemal, Standard enthalpy, entropy and Gibbs free energy of formation of «A» type carbonate phosphocalcium hydroxyapatites, J. Chem. Thermodyn. 106 (2017) 84–94.
[28] I. Olivas-Armendáriz, E. Santos-Rodríguez, M. Alvarado-Gutiérrez, Z. Meléndez-Molina, L. Márquez-Chávez, L. Valencia-Gómez, S. Martel-Estrada, Biocomposites scaffolds for bone tissue engineering, Int. J. Compos. Mater. 5 (2015) 167.
[29] A. Bannerman, R.L. Williams, S.C. Cox, L.M. Grover, Visualising phase change in a brushite-based calcium phosphate ceramic, Sci. Rep. 6 (2016) 1–10.
[30] B. León, J.A. Jansen, Thin Calcium Phosphate Coatings for Medical Implants, first ed., Springer Nature, New York, 2009.
[31] T. Furuhashi, I. Miksik, M. Smrz, B. Germann, D. Nebija, B. Lachmann, C. Noe, Comparison of aragonitic molluscan shell proteins, Comp. Biochem. Physiol. B 155 (2010) 195–200.
[32] P. Kyung Hee, K. Seok-Jae, J. Young-Hwa, M. Hyun-Joo, S. Ho-Jun, P. Yeong-Joon, Fabrication and biological properties of calcium phosphate/chitosan composite coating on titanium in modified SBF, Mater. Sci. Eng. C 90 (2018) 113–118.
[33] C. Ohtsuki, Y. Aoki, T. Kokubo, Y. Bando, M. Neo, T. Nakamura, Transmission electron microscopic observation of glass-ceramic A-W and apatite layer formed on its surface in a simulated body fluid, J. Ceram. Soc. Jpn. 103 (1995) 449–454.